JOURNAL OF SOLID STATE CHEMISTRY **131,** 54–63 (1997)
ARTICLE NO. SC977339

# Synthesis, Crystal Structure, and IR and Mössbauer Spectroscopy of the Isotypic Series $M_3Fe_2(SeO_3)_6 \cdot 2H_2O$ ($M$ = Mg, Co, Ni)

G. Giester and A. Beran

*Institut für Mineralogie und Kristallographie, Geozentrum, Universität Wien, Althanstraße 14, A-1090 Vienna, Austria*

and

G. J. Redhammer

*Institut für Mineralogie, Universität Salzburg, Hellbrunnerstraße 34, A-5020 Salzburg, Austria*

Received June 19, 1996; in revised form January 14, 1997; accepted February 5, 1997

**The representatives of the new isotypic series $M_3Fe_2(SeO_3)_6 \cdot 2H_2O$ ($M$ = Mg, Co, Ni) were prepared at 500 K from aqueous solutions, kept in Teflon-coated autoclaves. Their crystal structures were determined by direct methods from single-crystal X-ray diffraction data in the space group $P\bar{1}$ with $Z = 1$. $Mg_3Fe_2(SeO_3)_6 \cdot 2H_2O$: $a = 6.494(2)$, $b = 7.959(3)$, $c = 8.810(4)$ Å, $\alpha = 85.88(2)$, $\beta = 79.12(2)$, $\gamma = 76.09(2)^\circ$, $V = 433.9$ Å$^3$. $Co_3Fe_2(SeO_3)_6 \cdot 2H_2O$: $a = 6.520(2)$, $b = 7.995(3)$, $c = 8.774(4)$ Å, $\alpha = 85.51(2)$, $\beta = 78.77(1)$, $\gamma = 75.84(1)^\circ$, $V = 434.8$ Å$^3$. $Ni_3Fe_2(SeO_3)_6 \cdot 2H_2O$: $a = 6.474(2)$, $b = 7.943(3)$, $c = 8.736(4)$ Å, $\alpha = 85.37(1)$, $\beta = 78.51(1)$, $\gamma = 75.91(1)^\circ$, $V = 426.7$ Å$^3$. The three different $M$ sites are commonly occupied by $M^{2+}$ and $Fe^{3+}$ atoms in varying ratios. $MO_6$ octahedra are linked to each other by edges to build four-membered groups. Via common corners with further $MO_6$ octahedra and trigonal pyramidal $SeO_3$ groups, complex sheets parallel to (001) are formed which are interconnected by hydrogen bonds only. IR and Mössbauer spectra are discussed.** © 1997 Academic Press

## INTRODUCTION

In the past few years selenites of ferric iron have been the subject of detailed investigations; for a summary see (1) and literature cited therein. Recently, we have extended our studies to systems containing iron and selenium in addition to divalent cations, among them especially first row transition metal and earth alkaline elements. So far, the crystal structures of $Rb_4MFe_8(SeO_3)_{14}(SeO_2OH)_2 \cdot 2H_2O$ ($M$ = Mg, Cu) (2), $M_3Fe_2(SeO_3)_6$ ($M$ = Ca, Sr) (1), $ZnFe_2(SeO_3)_4$ (3), $M_3Fe_2(SeO_3)_6$ ($M$ = Cu, Zn) (4), and $Cu_3Fe_2(SeO_3)_6$-II (5) are known. The present paper describes synthesis, structural features, and IR and Mössbauer spectroscopy of the new compounds $M_3Fe_2(SeO_3)_6 \cdot 2H_2O$ ($M$ = Mg,Co,Ni), further denoted throughout the text as MGFE, COFE, and NIFE.

## EXPERIMENTAL PROCEDURES

*Sample preparation.* The starting materials for synthesis were $FeC_2O_4 \cdot 2H_2O$ and $SeO_2$, combined with $MgCO_3$, $Co(OH)_2$, or $Ni(OH)_2$. Aqueous solutions of these mixtures were filled (up to 50 vol%) in Teflon-coated steel autoclaves of 10 cm$^3$ capacity, heated to 500 K, kept at this temperature for several days, and finally cooled to room temperature within 12 h. In the course of this treatment the ferrous iron was completely oxidized, resulting in well-developed single crystals of Fe(III) oxysalts. The reaction products were separated from the mother liquid by filtering and washing with deionized water and acetone. Crystals of $Co_3(SeO_3)_3 \cdot H_2O$ and $Ni_3(SeO_3)_3 \cdot H_2O$ (6) were identified as coprecipitates of COFE and NIFE, respectively. The title compounds form tiny plates (up to 0.5 mm in diameter) flattened parallel to (001), which are commonly intergrown to clusters. Their colors are yellow (MGFE), dark purple–red (COFE), and brownish-orange (NIFE).

*Structure determination.* Single-crystal X-ray diffraction intensities were collected at room temperature on a Stoe AED2 four-circle diffractometer equipped with a graphite monochromator (Mo$K\alpha$ radiation, $2\theta$-$\omega$ scans; 40 steps per reflection, increased for $\alpha_1$–$\alpha_2$ splitting, $2 \times 4$ steps for background correction; 0.03° step width, 1–3 s per step; three standard reflections every 120 min; lattice parameters refined from 46–50 reflections in the $2\theta$ range 23°–42°). The results of the measurements and structure refinements as well as selected crystal data are summarized in Table 1. The measured intensities were corrected for Lorentz and polarization effects and for absorption by evaluation of $\psi$ scans. The crystal structure of COFE was determined by direct methods (7) and subsequent Fourier and difference Fourier syntheses. The atomic coordinates of COFE were used as a starting model in the refinements of MGFE and NIFE.



0022-4596/97 $25.00

**TABLE 1**
**Crystal Data and Details of the Intensity Measurements and Structure Refinements**

| | MGFE | COFE | NIFE |
|---|---|---|---|
| Space group | $P\bar{1}$ | $P\bar{1}$ | $P\bar{1}$ |
| $a$ [Å] | 6.494(2) | 6.520(2) | 6.474(2) |
| $b$ [Å] | 7.959(3) | 7.995(3) | 7.943(3) |
| $c$ [Å] | 8.810(4) | 8.774(4) | 8.736(4) |
| $\alpha$ [°] | 85.88(2) | 85.51(2) | 85.37(1) |
| $\beta$ [°] | 79.12(2) | 78.77(1) | 78.51(1) |
| $\gamma$ [°] | 76.09(2) | 75.84(1) | 75.91(1) |
| $V$ [Å$^3$] | 433.9 | 434.8 | 426.7 |
| $Z$ | 1 | 1 | 1 |
| $\rho_{calc}$ [gcm$^{-3}$] | 3.76 | 4.15 | 4.22 |
| $\mu$(Mo$K\alpha$) [cm$^{-1}$] | 144.7 | 171.0 | 178.1 |
| $2\theta_{max}$ [°] | 55 | 50 | 55 |
| Measured reflections | 4002 | 3086 | 4189 |
| Unique data set | 2000 | 1543 | 1980 |
| Data with $F_0 > 4\sigma(F_0)$ | 1628 | 1102 | 1588 |
| Variables | 156 | 156 | 156 |
| Min/max transmission | 0.05–0.15 | 0.09–0.25 | 0.06–0.65 |
| Extinction coefficient | 0.003(1) | 0.001(1) | 0.002(1) |
| $R1$ [for $F_0 > 4\sigma(F_0)$] | 0.028 | 0.037 | 0.037 |
| $wR2$ [for all $F_0^2$] | 0.070 | 0.088 | 0.109 |
| $R1 = \sum\|\|F_0\| - \|F_c\|\|/\sum\|F_0\|$ | | | |
| $wR2 = [\sum w(F_0^2 - F_c^2)^2/\sum wF_0^4]^{1/2}$ | | | |
| $w = 1/[\sigma^2(F_0^2) + (a \times P)^2]$ | $a = 0.041$ | 0.051 | 0.084 |
| $P = \{[\max \text{ of } (0 \text{ or } F_0^2)] + 2F_c^2\}/3$ | | | |

Final structure parameters of the title compounds, obtained by full-matrix least-squares techniques on $F^2$ (SHELXL-93 (8)), are listed in Table 2; selected interatomic distances and bond angles are given in Table 3. The hydrogen atoms, located by difference Fourier maps, were refined by restricting the O–H and H1–H2 distances to 0.90(2) and 1.44(5) Å, respectively. The $M^{2+}/Fe^{3+}$ ratios of the cation sites $M1$–3 were refined individually, restricting the total ratio to be 3 : 2 and all sites to be fully occupied.

*TG measurements.* TGA investigations were performed on a computer-controlled Mettler M3 microbalance combined with a TA 4000 Thermo Analysis System. Fine grained crystals of MGFE (4.681 mg), COFE (1.178 mg), and NIFE (11.698 mg) were heated under nitrogen atmosphere in the temperature range from 30 to 800°C with a heating rate of 2°C min$^{-1}$. Thermal decomposition (Fig. 1; Table 4) took place in several steps, the first of which could be attributed to the total loss of $2H_2O$ pfu. In MGFE, and also weakly indicated in COFE, two further steps infered the release of each $3SeO_2$ pfu, while in NIFE the total content of $6SeO_2$ pfu was released in a single step. The final decomposition products were identified by X-ray powder diffraction (Philips PW3020 diffractometer, Cu$K\alpha$ radiation) to be mixtures of $M^{2+}O$ (halite type) and $M^{2+}Fe_2O_4$ (spinel type).

*Chemical analyses.* The chemical compositions of the title compounds were investigated by EDX analysis at 20 kV operating voltage, using a Jeol JSM-6400 scanning electron microscope with the program system LINK eXL10 (in the case of MGFE, a peak overlap (Mg/Se) allowed only qualitative results). Further analyses were performed with an ARL-SEMQ electron microprobe; operation conditions were 15 kV acceleration potential and about 15 nA sample

**TABLE 2**
**Atomic Coordinates and Anisotropic Displacement Parameters with e.s.d.'s in Parentheses**

| | $x$ | $y$ | $z$ | $U_{eqv}$ | $U_{11}$ | $U_{22}$ | $U_{33}$ | $U_{23}$ | $U_{13}$ | $U_{12}$ |
|---|---|---|---|---|---|---|---|---|---|---|
| | | | | | MGFE | | | | | |
| $M1$ | 0.5 | 0.5 | 0.5 | 0.0132(4) | 0.0121(6) | 0.0132(6) | 0.0134(7) | 0.0004(4) | − 0.0027(5) | − 0.0011(4) |
| $M2$ | 0.3119(2) | 0.17696(14) | 0.76442(15) | 0.0146(3) | 0.0113(6) | 0.0153(6) | 0.0166(7) | − 0.0001(4) | − 0.0025(5) | − 0.0019(4) |
| $M3$ | 0.13709(14) | 0.89596(11) | 0.61711(12) | 0.0127(3) | 0.0101(5) | 0.0132(5) | 0.0142(5) | 0.0007(3) | − 0.0020(4) | − 0.0021(3) |
| Se1 | 0.20213(6) | 0.71097(5) | 0.27016(5) | 0.01118(13) | 0.0081(2) | 0.0119(2) | 0.0125(2) | 0.00046(15) | − 0.0023(2) | − 0.00007(14) |
| Se2 | 0.32997(6) | 0.20427(5) | 0.36750(5) | 0.01008(12) | 0.0068(2) | 0.0105(2) | 0.0123(2) | 0.00130(14) | − 0.0016(2) | − 0.00126(14) |
| Se3 | 0.23539(7) | 0.57535(5) | 0.87105(5) | 0.01282(13) | 0.0122(2) | 0.0128(2) | 0.0123(2) | 0.0002(2) | − 0.0009(2) | − 0.00196(14) |
| O1 | 0.2308(5) | 0.6948(4) | 0.4633(4) | 0.0153(7) | 0.0158(15) | 0.0136(14) | 0.013(2) | 0.0034(12) | − 0.0022(13) | 0.0013(11) |
| O2 | 0.3997(5) | 0.8096(4) | 0.1873(4) | 0.0175(7) | 0.0109(15) | 0.023(2) | 0.018(2) | 0.0030(13) | − 0.0009(13) | − 0.0035(12) |
| O3 | − 0.0202(5) | 0.8747(4) | 0.2640(4) | 0.0124(6) | 0.0092(13) | 0.0124(13) | 0.015(2) | 0.0005(11) | − 0.0025(12) | − 0.0002(10) |
| O4 | 0.1714(5) | 0.0628(4) | 0.4289(4) | 0.0124(6) | 0.0103(13) | 0.0143(13) | 0.014(2) | 0.0035(11) | − 0.0030(12) | − 0.0057(11) |
| O5 | 0.5791(5) | 0.0671(4) | 0.3342(4) | 0.0143(6) | 0.0078(14) | 0.0124(13) | 0.022(2) | − 0.0006(1) | 0.0030(13) | − 0.0003(11) |
| O6 | 0.3379(5) | 0.2956(4) | 0.5352(4) | 0.0135(6) | 0.0135(14) | 0.0167(14) | 0.011(2) | − 0.0022(11) | − 0.0017(12) | − 0.0042(11) |
| O7 | 0.1351(5) | 0.4064(4) | 0.8504(4) | 0.0182(7) | 0.015(2) | 0.0159(14) | 0.024(2) | − 0.0027(13) | − 0.0018(14) | − 0.0055(12) |
| O8 | 0.0621(5) | 0.7452(4) | 0.8012(4) | 0.0196(7) | 0.015(2) | 0.0157(14) | 0.024(2) | 0.0036(13) | − 0.0003(14) | 0.0005(12) |
| O9 | 0.4458(5) | 0.5547(4) | 0.7196(4) | 0.0150(6) | 0.0104(14) | 0.0184(15) | 0.015(2) | − 0.0021(12) | 0.0026(13) | − 0.0031(11) |
| O10 | 0.2562(6) | 0.0681(5) | 0.9852(4) | 0.0259(8) | 0.019(2) | 0.032(2) | 0.016(2) | 0.0074(15) | 0.0025(15) | 0.0085(14) |
| H1 | 0.172(10) | 0.145(7) | 0.047(7) | 0.06(2) | | | | | | |
| H2 | 0.308(11) | − 0.032(5) | 0.030(8) | 0.06(2) | | | | | | |

**TABLE 2**—*Continued*

| | $x$ | $y$ | $z$ | $U_{eqv}$ | $U_{11}$ | $U_{22}$ | $U_{33}$ | $U_{23}$ | $U_{13}$ | $U_{12}$ |
|---|---|---|---|---|---|---|---|---|---|---|
| | | | | | COFE | | | | | |
| *M*1 | 0.5 | 0.5 | 0.5 | 0.0133(4) | 0.0098(8) | 0.0088(8) | 0.0200(10) | 0.0016(7) | − 0.0033(7) | − 0.0001(6) |
| *M*2 | 0.3133(2) | 0.17781(14) | 0.76099(15) | 0.0134(3) | 0.0078(6) | 0.0093(6) | 0.0216(7) | 0.0011(5) | − 0.0016(5) | − 0.0006(5) |
| *M*3 | 0.1375(2) | 0.89621(14) | 0.61695(14) | 0.0128(3) | 0.0066(6) | 0.0086(6) | 0.0218(7) | 0.0016(5) | − 0.0019(5) | − 0.0002(4) |
| Se1 | 0.20156(13) | 0.70907(11) | 0.26965(11) | 0.0135(2) | 0.0076(4) | 0.0099(4) | 0.0210(5) | 0.0008(3) | − 0.0036(3) | 0.0023(3) |
| Se2 | 0.32981(12) | 0.20478(10) | 0.36606(10) | 0.0118(2) | 0.0053(4) | 0.0080(4) | 0.0204(5) | 0.0020(3) | − 0.0014(3) | 0.0004(3) |
| Se3 | 0.23784(13) | 0.57235(11) | 0.87502(11) | 0.0148(3) | 0.0108(4) | 0.0112(5) | 0.0209(5) | 0.0002(4) | − 0.0011(3) | − 0.0010(3) |
| O1 | 0.2311(9) | 0.6940(8) | 0.4601(7) | 0.0157(13) | 0.012(3) | 0.014(3) | 0.018(3) | 0.004(2) | − 0.001(2) | 0.001(2) |
| O2 | 0.4000(9) | 0.8078(8) | 0.1848(8) | 0.0203(14) | 0.009(3) | 0.019(3) | 0.030(4) | 0.006(3) | 0.002(3) | − 0.003(3) |
| O3 | − 0.0187(9) | 0.8745(7) | 0.2618(7) | 0.0153(13) | 0.008(3) | 0.010(3) | 0.026(4) | − 0.003(3) | − 0.007(2) | 0.006(2) |
| O4 | 0.1737(9) | 0.0634(7) | 0.4265(7) | 0.0150(13) | 0.007(3) | 0.011(3) | 0.027(4) | 0.004(2) | − 0.002(2) | − 0.004(2) |
| O5 | 0.5790(8) | 0.0677(7) | 0.3297(7) | 0.0125(12) | 0.005(3) | 0.010(3) | 0.019(3) | − 0.001(2) | − 0.002(2) | 0.004(2) |
| O6 | 0.3385(9) | 0.2950(7) | 0.5357(7) | 0.0164(13) | 0.014(3) | 0.010(3) | 0.024(4) | 0.001(3) | − 0.001(3) | − 0.003(2) |
| O7 | 0.1354(9) | 0.4044(8) | 0.8503(8) | 0.0201(14) | 0.015(3) | 0.011(3) | 0.034(4) | − 0.001(3) | − 0.003(3) | − 0.003(3) |
| O8 | 0.0613(9) | 0.7438(8) | 0.8078(8) | 0.0205(14) | 0.013(3) | 0.011(3) | 0.032(4) | 0.001(3) | 0.000(3) | 0.005(2) |
| O9 | 0.4490(9) | 0.5543(7) | 0.7260(7) | 0.0163(13) | 0.014(3) | 0.012(3) | 0.020(4) | 0.004(2) | − 0.002(3) | − 0.001(3) |
| O10 | 0.2502(12) | 0.0686(9) | 0.9857(8) | 0.034(2) | 0.036(4) | 0.029(4) | 0.019(4) | 0.004(3) | − 0.001(3) | 0.019(3) |
| H1 | 0.200(17) | 0.129(11) | 0.072(7) | 0.04(2) | | | | | | |
| H2 | 0.311(16) | − 0.039(5) | 0.016(11) | 0.04(2) | | | | | | |
| | | | | | NIFE | | | | | |
| *M*1 | 0.5 | 0.5 | 0.5 | 0.0092(3) | 0.0109(5) | 0.0087(6) | 0.0071(6) | − 0.0007(4) | − 0.0013(4) | − 0.0004(4) |
| *M*2 | 0.30976(13) | 0.17589(11) | 0.75963(10) | 0.0094(2) | 0.0102(4) | 0.0093(4) | 0.0079(5) | − 0.0009(3) | − 0.0007(3) | − 0.0011(3) |
| *M*3 | 0.13552(12) | 0.89787(10) | 0.61546(10) | 0.0090(2) | 0.0095(4) | 0.0092(4) | 0.0079(4) | − 0.0007(3) | − 0.0013(3) | − 0.0015(3) |
| Se1 | 0.20323(9) | 0.70903(8) | 0.27230(8) | 0.0108(2) | 0.0118(3) | 0.0111(3) | 0.0084(3) | − 0.0020(2) | − 0.0033(2) | 0.0011(2) |
| Se2 | 0.33029(9) | 0.20594(8) | 0.36788(7) | 0.0087(2) | 0.0091(3) | 0.0091(3) | 0.0073(3) | − 0.0002(2) | − 0.0014(2) | − 0.0015(2) |
| Se3 | 0.23732(9) | 0.57074(8) | 0.87525(7) | 0.0113(2) | 0.0131(3) | 0.0116(3) | 0.0083(3) | − 0.0021(2) | − 0.0002(2) | − 0.0021(2) |
| O1 | 0.2288(7) | 0.6942(6) | 0.4643(6) | 0.0119(9) | 0.014(2) | 0.009(2) | 0.010(2) | − 0.001(2) | − 0.004(2) | 0.002(2) |
| O2 | 0.4047(7) | 0.8098(6) | 0.1841(6) | 0.0171(10) | 0.014(2) | 0.024(3) | 0.014(3) | 0.006(2) | − 0.005(2) | − 0.006(2) |
| O3 | − 0.0176(6) | 0.8758(6) | 0.2604(5) | 0.0106(8) | 0.011(2) | 0.010(2) | 0.009(2) | − 0.001(2) | − 0.002(2) | 0.001(2) |
| O4 | 0.1719(7) | 0.0622(5) | 0.4277(5) | 0.0091(8) | 0.010(2) | 0.006(2) | 0.011(2) | − 0.001(2) | − 0.002(2) | − 0.001(1) |
| O5 | 0.5822(7) | 0.0680(6) | 0.3310(6) | 0.0124(9) | 0.010(2) | 0.014(2) | 0.012(2) | − 0.004(2) | − 0.001(2) | 0.000(2) |
| O6 | 0.3373(7) | 0.2955(6) | 0.5394(6) | 0.0122(9) | 0.015(2) | 0.010(2) | 0.012(2) | − 0.003(2) | 0.000(2) | − 0.004(2) |
| O7 | 0.1342(7) | 0.4014(6) | 0.8535(6) | 0.0193(10) | 0.016(2) | 0.016(2) | 0.026(3) | − 0.004(2) | 0.000(2) | − 0.006(2) |
| O8 | 0.0584(7) | 0.7446(6) | 0.8057(6) | 0.0176(10) | 0.016(2) | 0.018(2) | 0.013(2) | 0.008(2) | 0.002(2) | 0.001(2) |
| O9 | 0.4497(7) | 0.5531(6) | 0.7257(6) | 0.0140(9) | 0.015(2) | 0.015(2) | 0.010(2) | 0.001(2) | 0.000(2) | − 0.003(2) |
| O10 | 0.2438(9) | 0.0620(8) | 0.9834(6) | 0.0293(13) | 0.034(3) | 0.034(3) | 0.008(3) | 0.003(2) | 0.003(2) | 0.008(3) |
| H1 | 0.147(19) | 0.131(13) | 0.055(12) | 0.10(4) | | | | | | |
| H2 | 0.278(22) | − 0.044(8) | 0.028(14) | 0.10(4) | | | | | | |

*Note.* The anisotropic displacement parameter is defined as $\exp(-2\pi^2\sum_i\sum_j U_{ij}h_ih_j\boldsymbol{a}_i^*\boldsymbol{a}_j^*)$

current. During measurement, partial decomposition of the polished crystal surfaces was observed. The quantitative results of chemical analyses, compiled in Table 5, have therefore to be interpreted with necessary care and are considered not to be in contradiction with the formulas derived from the crystal structure analyses.

*IR spectroscopy.* Single crystals with maximum thickness of about 20 μm were isolated for the FTIR spectroscopic examination. Single-crystal spectra were recorded with a resolution of 4 $cm^{-1}$ in the 4000–1000 $cm^{-1}$ region on a Perkin–Elmer FTIR microscope using 0.60 numerical aperture Cassegrains and a liquid-nitrogen-cooled MCT detector, combined with a Perkin–Elmer FTIR spectrometer 1760X. Measuring spots were chosen according to the dimensions of optically clear crystal parts varying from $40\times40$ to $90\times90$ μm. Powder spectra were recorded from 5500 to 420 $cm^{-1}$ on the same FTIR spectrometer equipped with a TGS detector and a microfocus accessory designed for the measurement of the prepared KBr microdisks. Data handling and calculations were managed by the program IRDM (Perkin–Elmer). The single-crystal spectra are presented in Fig. 2a and the 1000–420 $cm^{-1}$ region of the powder spectra is shown in Fig. 2b. Wavenumber values of significant absorption maxima are summarized in Table 6.

**TABLE 3**
**Selected Interatomic Distances [Å] and Angles**

| | MGFE | COFE | NIFE |
|---|---|---|---|
| $M1$–O9 (2×) | 1.962(4) | 2.010(6) | 1.996(5) |
| $M1$–O1 (2×) | 2.098(3) | 2.104(6) | 2.093(4) |
| $M1$–O6 (2×) | 2.116(3) | 2.128(6) | 2.113(4) |
| ⟨$M1$–O⟩ | ⟨2.059⟩ | ⟨2.081⟩ | ⟨2.067⟩ |
| $M^{2+}$: $Fe^{3+}$ | 46 : 54 | ≈ (84 : 16) | ≈ (74 : 26) |
| $\Delta_{oct}$ | 0.00112 | 0.00060 | 0.00061 |
| $M2$–O7 | 2.022(3) | 2.020(6) | 2.012(5) |
| $M2$–O2 | 2.025(4) | 2.048(6) | 2.036(5) |
| $M2$–O10 | 2.075(4) | 2.100(7) | 2.096(6) |
| $M2$–O5 | 2.093(3) | 2.082(6) | 2.058(5) |
| $M2$–O3 | 2.095(3) | 2.112(6) | 2.074(4) |
| $M2$–O6 | 2.162(4) | 2.115(6) | 2.071(5) |
| ⟨$M2$–O⟩ | ⟨2.079⟩ | ⟨2.080⟩ | ⟨2.058⟩ |
| $M^{2+}$: $Fe^{3+}$ | 73 : 27 | ≈ (54 : 46) | ≈ (45 : 55) |
| $\Delta_{oct}$ | 0.00052 | 0.00028 | 0.00018 |
| $M3$–O8 | 2.003(4) | 2.047(6) | 2.033(5) |
| $M3$–O5 | 2.060(3) | 2.082(6) | 2.058(4) |
| $M3$–O4 | 2.061(3) | 2.070(6) | 2.025(5) |
| $M3$–O4 | 2.063(3) | 2.081(6) | 2.043(4) |
| $M3$–O1 | 2.074(3) | 2.102(6) | 2.068(5) |
| $M3$–O3 | 2.077(3) | 2.093(6) | 2.076(4) |
| ⟨$M2$–O⟩ | ⟨2.056⟩ | ⟨2.079⟩ | ⟨2.051⟩ |
| $M^{2+}$: $Fe^{3+}$ | 54 : 46 | ≈ (54 : 46) | ≈ (68 : 32) |
| $\Delta_{oct}$ | 0.00014 | 0.00007 | 0.00008 |
| Se1–O1 | 1.739(4) | 1.710(6) | 1.710(5) |
| Se1–O2 | 1.686(3) | 1.698(6) | 1.716(4) |
| Se1–O3 | 1.703(3) | 1.706(5) | 1.710(5) |
| ⟨Se1–O⟩ | ⟨1.709⟩ | ⟨1.705⟩ | ⟨1.712⟩ |
| O1–Se1–O2 | 102.2(2) | 101.7(3) | 102.8(2) |
| O1–Se1–O3 | 104.3(2) | 104.7(3) | 105.3(2) |
| O2–Se1–O3 | 101.0(2) | 100.2(3) | 99.4(2) |
| ⟨O–Se1–O⟩ | ⟨102.5⟩ | ⟨102.2⟩ | ⟨102.5⟩ |
| Se2–O4 | 1.697(3) | 1.689(6) | 1.700(4) |
| Se2–O5 | 1.707(3) | 1.710(5) | 1.715(4) |
| Se2–O6 | 1.707(3) | 1.720(6) | 1.722(5) |
| ⟨Se2–O⟩ | ⟨1.704⟩ | ⟨1.706⟩ | ⟨1.712⟩ |
| O4–Se2–O5 | 101.2(2) | 100.9(3) | 100.9(2) |
| O4–Se2–O6 | 102.7(2) | 103.3(3) | 103.3(2) |
| O5–Se2–O6 | 101.0(2) | 101.4(3) | 101.4(2) |
| ⟨O–Se2–O⟩ | ⟨101.6⟩ | ⟨101.9⟩ | ⟨101.9⟩ |
| Se3–O7 | 1.664(3) | 1.685(6) | 1.679(5) |
| Se3–O8 | 1.698(3) | 1.708(6) | 1.728(5) |
| Se3–O9 | 1.706(3) | 1.690(6) | 1.684(5) |
| ⟨Se3–O⟩ | ⟨1.689⟩ | ⟨1.694⟩ | ⟨1.697⟩ |
| O7–Se3–O8 | 103.6(2) | 102.6(3) | 102.9(2) |
| O7–Se3–O9 | 102.1(2) | 102.6(3) | 103.1(2) |
| O8–Se3–O9 | 98.9(2) | 100.1(3) | 99.8(2) |
| ⟨O–Se3–O⟩ | ⟨101.5⟩ | ⟨101.8⟩ | ⟨101.9⟩ |

*Note.* Refined cation distributions for the $M1$–3 sites. Bond-length distortions $\Delta_{oct}$ defined as $\Delta_{oct} = 1/6\sum[(d_i - d_m)/d_m]^2$.

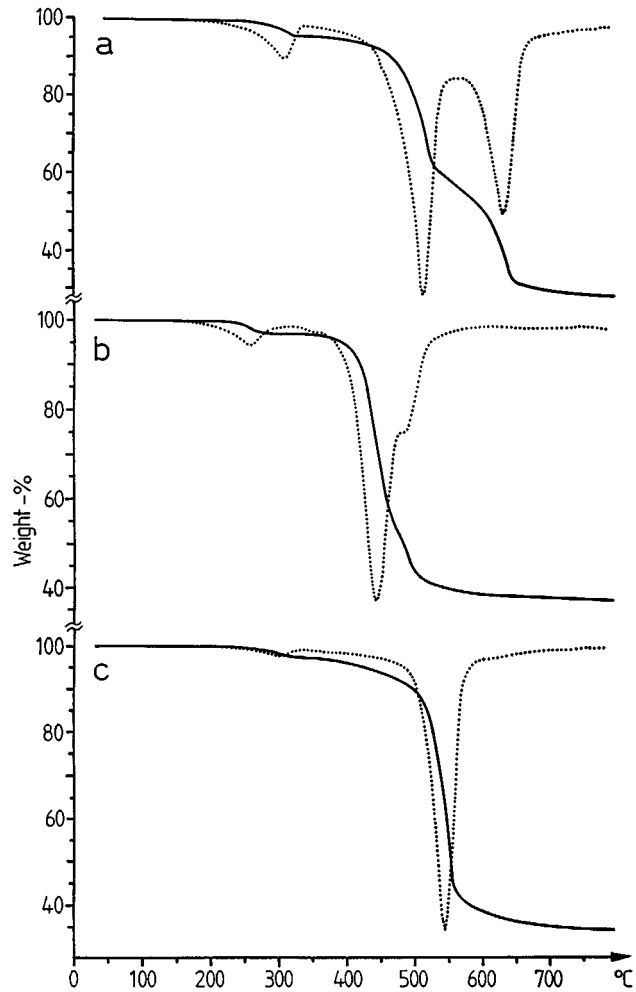


**FIG. 1.** TGA curves for (a) MGFE, (b) COFE, and (c) NIFE. The weight losses (full lines) and first derivatives (dotted lines) are shown.

*Mössbauer spectroscopy.* $^{57}$Fe Mössbauer spectra of MGFE and NIFE were recorded at 298 K using a conventional Mössbauer apparatus (Halder Elektronik GmbH) in constant acceleration mode, symmetrical triangular movement of the 50 mCi $^{57}$Co/Rh source, and 1024 MCA. A detailed description of a similar experimental setup is given in (9). The spectrometer velocity scale was calibrated to α-Fe and the two symmetrical spectra obtained were folded to 510 channels. The raw spectra were refined using symmetrical doublets with Lorentzian lineshape using the program MOESALZ (10). Refined Mössbauer spectra of MGFE and NIFE are represented in Figs. 3a and 3b, and the Mössbauer parameters are compiled in Table 7.

## RESULTS AND DISCUSSION

*Crystal structure.* The new structure type of $M_3Fe_2(SeO_3)_6 \cdot 2H_2O$ ($M$ = Mg, Co, Ni) is characterized by

**TABLE 4**
**Details of TGA Measurements for MGFE, COFE, and NIFE**

| | MGFE | | | COFE | | | NIFE | | |
|---|---|---|---|---|---|---|---|---|---|
| | Calc. | Obs. | $T$ [°C] | Calc. | Obs. | $T$ [°C] | Calc. | Obs. | $T$ [°C] |
| $-2H_2O$ | 3.46% | 3.77% | 250–315 (300) | 3.32% | 2.9% | 200–310 (255) | 3.32% | 3.11% | 220–370 (300) |
| $-6SeO_2$ | 67.76% | 67.63% | (510, 630) | 61.29% | 60.3% | (445, 485) | 61.33% | 62.32% | (545) |
| Total loss | 71.43% | 71.40% | 30–800 | 64.60% | 63.2% | 30–800 | 64.65% | 65.43% | 30–800 |

*Note.* Maxima of first derivative in parentheses.

complex polyhedral sheets parallel to (001), which are linked by hydrogen bonds only as illustrated in Figs. 4 and 5. This atomic arrangement explains the morphology of the crystals and their perfect cleavage parallel to (001). The sheets are formed by the linkage of $MO_6$ octahedra and $SeO_3$ groups as follows: a centrosymmetric, basal unit is built up by the edge linkages of four $MO_6$ octahedra of the sequence $M2$–$M3$–$M3$–$M2$. This group is connected via common corners to $M(1)O_6$ octahedra and $SeO_3$ trigonal pyramids (Se1 to Se3) to an infinite sheet complex parellel to (0 0 1).

The $SeO_3$ groups have mean $\langle$Se–O$\rangle$ and $\langle$O–Se–O$\rangle$ values ranging from 1.69 to 1.71 Å and 101.5° to 102.5°, respectively, which comply well with data reported in the literature. The selenite groups show moderate bond-lengths and bond-angle distortions which generally are analogous for specific sites of the title compounds. This finding is also true for corresponding $MO_6$ octahedra: the centrosymmetric $M(1)$O6 polyhedra are less bond-angle distorted while the common edges within the four-membered octahedral groups cause stronger distortions. Nonopposite O–$M$–O angles and O–O contacts of the individual polyhedra are in the ranges (in order MGFE/COFE/NIFE) 84.1°–95.9°/84.2°–95.8°/84.3°–95.7° and 2.77–3.13/2.79–3.14/2.79–3.12 Å for $M(1)$; 79.1°–99.2°/79.4°–100.4°/79.8°–100.2° and 2.67–3.19/2.68–3.20/2.65–3.15 Å for $M(2)$; and 80.3°–104.9°/79.8°–105.9°/79.7°–105.6° and 2.67–3.28/2.68–3.34/2.65–3.29 Å for $M(3)$. The oxygen atoms O1 and O3–O6 have a nearly planar to slightly pyramidal coordination to one selenium and to two $M$ atoms, O2 and O7–O9 are 2-coordinated to one Se and $M$ atom each. Consequently, individual oxygen–cation distances are shorter for the latter ones in order to maintain well-balanced bond strengths. The O10 atom, which forms the $H_2O$ molecule, is only bound to one $M(2)$ atom, the next-nearest $M$ cations are as far as 3.8–3.9 Å.

*Cation site distribution and Mössbauer spectroscopy.* Despite of the fact that the crystal structure type consists of three different $MO_6$ sites, the divalent cations and ferric iron are not separated but distributed with varying cation $M^{2+}/Fe^{3+}$ ratios among these positions. These cation ratios can be deduced from the mean $M$–O bond lengths and further from the refinement of the respective occupancy factors of the individual sites $M1$ to $M3$. The scattering

**TABLE 5**
**Chemical Composition (wt% of Elements) for MGFE, COFE, and NIFE by Microprobe (I) and by EDX (II) Analysis**

| | MGFE | | COFE | | | NIFE | | |
|---|---|---|---|---|---|---|---|---|
| | Calc. | Obs. I | Calc. | Obs. I | II | Calc. | Obs. I | II |
| $M$ | 7.42 | 8.4/— | 16.27 | 16.0/15.0 | | 16.22 | 14.7/18.4 | |
| Fe | 11.37 | 9.7/— | 10.28 | 9.4/10.3 | | 10.29 | 7.5/6.4 | |
| Se | 48.22 | 47.7/— | 43.61 | 42.4/41.3 | | 43.64 | 40.0/40.8 | |
| H | 0.41 | 0.45 | 0.37 | 0.32 | | 0.37 | 0.35 | |

*Note.* H contents calculated from TGA measurements.

**TABLE 6**
**Band Assignment of the IR Absorption Spectra in MGFE, COFE, and NIFE**

| | MGFE | COFE | NIFE |
|---|---|---|---|
| $H_2O$ stretching ($\nu_3 + \nu_1$) | 3486 | 3476 | 3466 |
| | 3373 | 3340 sh | 3330 sh |
| | 3258 | 3194 | 3125 |
| | ~ 2900 sh | ~ 2850 sh | ~ 2900 sh |
| $H_2O$ bending $\nu_2$ | 1674 | 1656 | 1662 |
| | 1632 | 1615 | 1594 |
| | 1592 sh | | |
| Lattice overtones | 1231 | 1235 | 1242 |
| | 1132 | 1114 | 1111 |
| | 1112 | — | 1091 |
| $SeO_3$ stretching symmetric $\nu_1$ | 845 | 844 sh | 847 sh |
| | 813 | 815 | 816 |
| $SeO_3$ stretching asymmetric $\nu_3$ | 790 | 759 | 768 |
| | 728 | 700 | 718 |
| | 670 | 640 | 647 |
| $MO_6$ stretching | 517 | 511 | 526 |
| | 495 sh | 490 sh | 499 sh |

*Note.* Wave number values in the 4000–1000 $cm^{-1}$ region deduced from single-crystal spectra, in the 1000–420 $cm^{-1}$ range from powder spectra

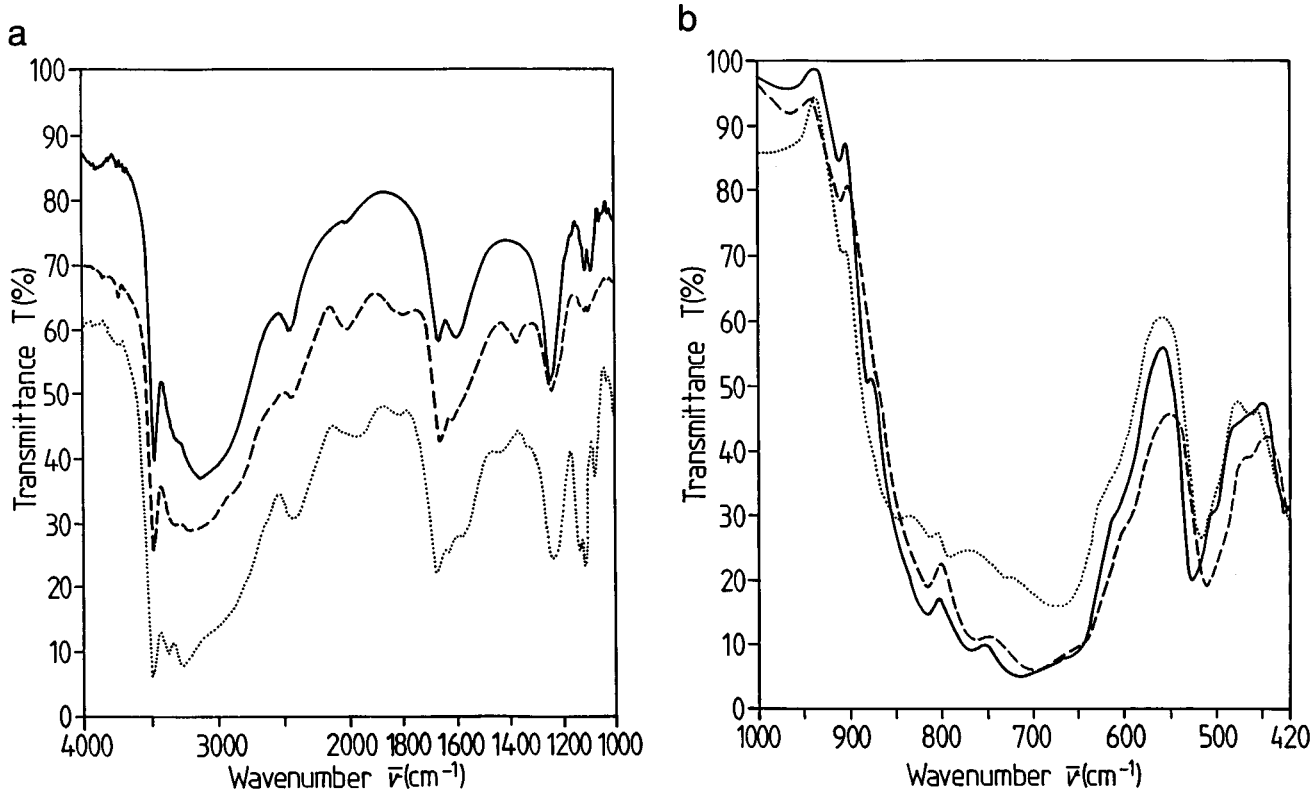


**FIG. 2.** IR absorption spectra of MGFE (dotted), COFE (dashed), and NIFE (continuous line drawing) of (a) single-crystal parallel to (001) in the 4000–1000 cm$^{-1}$ region and (b) KBr pellets in the 1000–420 cm$^{-1}$ region.

strength of Fe similar to Co or Ni allows rough estimations only in COFE and NIFE, while for MGFE the refinement of the Mg/Fe cation distribution is rather accurate. The Mg atoms preferably occupy the $M(2)O_6$ octahedron, which is in agreement with the somewhat larger mean $M(2)$–O distance. The Co and Ni atoms, on the other hand, seem to prefer the centrosymmetric $M(1)O_6$ polyhedron.

The Mössbauer spectra of both compounds consist of two asymmetrically broadened narrow-split resonance absorption peaks. When the high-velocity region (1.5–

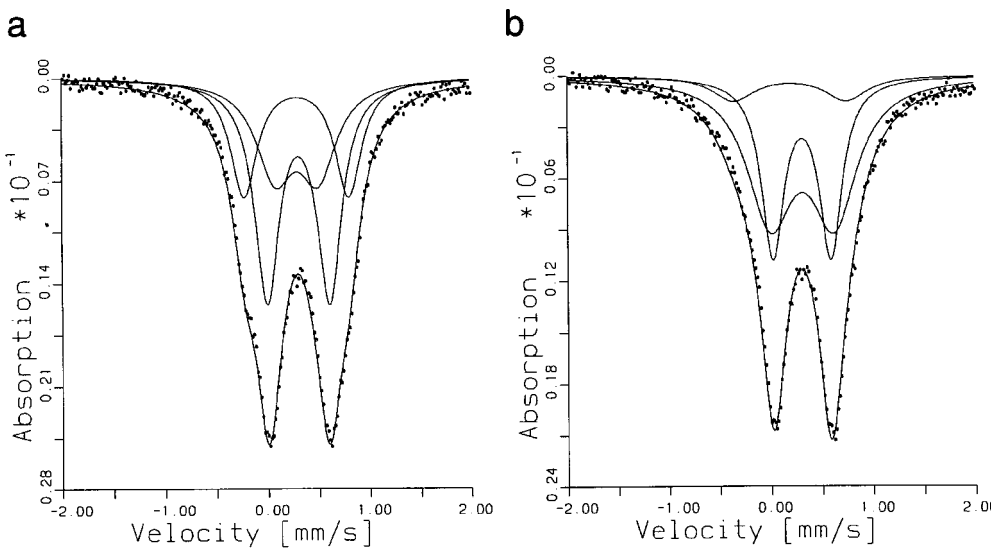


**FIG. 3.** Refined $^{57}$Fe Mössbauer spectra of MGFE (a) and NIFE (b) collected at 298 K.

**TABLE 7**
**$^{57}$Fe Mössbauer Hyperfine Parameters and Relative Area Ratios Derived from Mössbauer Spectroscopy for MGFE and NIFE**

| | MGFE | | NIFE | |
|---|---|---|---|---|
| *M*1 | | | | |
| $\delta^a$ | 0.393 | 0.392 | 0.342 | 0.297 |
| $\Delta^b$ | 0.988 | 1.016 | 1.138 | 1.093 |
| $\Gamma^c$ | 0.36 | 0.314 | 0.50 | 0.492 |
| $A^d$ | 27 | 26 | 14 | 10 |
| *M*2 | | | | |
| $\delta$ | 0.407$^e$ | 0.394 | 0.413$^e$ | 0.412 |
| $\Delta$ | 0.565$^e$ | 0.423 | 0.566$^e$ | 0.559 |
| $\Gamma$ | 0.36$^e$ | 0.440 | 0.360$^e$ | 0.266 |
| $A$ | 73$^e$ | 29 | 86$^e$ | 35 |
| *M*3 | | | | |
| $\delta$ | — | 0.409 | — | 0.416 |
| $\Delta$ | — | 0.603 | — | 0.617 |
| $\Gamma$ | — | 0.290 | — | 0.544 |
| $A$ | — | 45 | — | 55 |
| $\chi^f$ | 0.439 | 0.360 | 0.488 | 0.455 |

[a] Isomer shift [mm/s] $\pm$ 0.02 mm/s.
[b] Quadrupole splitting [mm/s] $\pm$ 0.02 mm/s.
[c] Full width at half maximum [mm/s] $\pm$ 0.02 mm/s.
[d] Realtive area ratio [%] $\pm$ 2%.
[e] Parameters correspond to a not splitted $M2 + M3$ site.
[f] Chi quadrat parameter.

2.5 mm/s) was examined, no evidence for further resonance absorption was found, which means that no ferrous iron is present in both samples. The nonsymmetric shape of the spectra exhibits the presence of two well-separated ferric iron subcomponents, having distinct different quadrupole splittings (QS) and slightly different isomer shifts (IS). Using such a two-doublet model, the spectra could be well refined, the corresponding hyperfine parameters are included in Table 7. On the basis of the variation of individual *M*–O distances with respect to mean *M*–O values (polyhedral bond length distortion, Table 3), the outer ferric doublet was dedicated to the *M*1 site and the inner to the not separated $M2 + M3$ sites. As we deal with $Fe^{3+}$ ions in rather similar octahedral sites only, the recoilless Mössbauer fraction *f* can be assumed to be equal for all three sites. Thus an extraction of quantitative area ratios can be done at room temperature. The relative area ratios for ferric iron, derived from Mössbauer spectroscopy, do agree very well with the site occupation factors from crystal structure refinement: using a two-doublet model, 27% of total iron occupies the *M*1 position in MGFE, whereas 14% is found on *M*1 in NIFE.

Splitting the inner doublet into two components (*M*2, *M*3) leads to somewhat better fits (lower $\chi^2$ values), however the difference in hyperfine parameters of these two new doublets in a three-doublet model are rather low, especially for NIFE, where QS values differ from each other only by 0.08 mm/s. Furthermore, the IS of the innermost doublet had to be fixed to a reliable value during the fitting procedure. For MGFE, three-doublet refinements converge better; here the difference in QS between individual doublets is larger. The dedication of subcomponents in the three-doublet model was predominantly done on the basis of site occupation factors, derived from single crystal work, rather than on site distortions.

In MGFE (Fig. 3a) the relative area ratios of the individual components in the three-doublet fit are 26, 29, and 45% for the outer to inner doublet, respectively. The doublet with a QS of 1.02 mm/s and an $A = 26\%$ was assigned to the *M*1 site, which shows the largest $\Delta_{oct} = 0.00112$, in accordance with the general finding that the QS of $Fe^{3+}$ is positively correlated with polyhedral distortion. The doublet with a QS of 0.42 mm/s and an area ratio of 29% was dedicated to the *M*2 site and the doublet with a QS of 0.60 mm/s and a relative area ratio of 45% to the *M*3 site, in some contradiction to what would be expected from $\Delta_{oct}$ values. Nevertheless, as there is such good agreement between area ratios derived from Mössbauer spectroscopy and site occupation factors in the structure refinement, this doublet assignment seems to be justified. For NIFE (Fig. 3b), as in the two-doublet model and in MGFE, the doublet with a QS of 1.09 mm/s and $A = 10\%$ was assigned to the most distorted site (*M*1) and the two doublets with QS of 0.56 mm/s and $A = 35\%$ and QS of 0.62 mm/s and $A = 55\%$ were generally assigned to the *M*2 and *M*3 sites.

The $^{57}$Fe Mössbauer hyperfine parameters are typical for $Fe^{3+}$ in octahedral coordination. The size of quadrupole splittings suggests slight to moderate distortions of octahedra. The isomershift values are rather similar, except that of *M*1 in NIFE, which is distinctly lower. This might indicate a minor difference in the covalent character of *M*–O bonding compared to *M*2 and *M*3.

*The hydrogen bonding system and IR spectroscopy.* The $H_2O$ system (Table 8, Fig. 5), exclusively linking the individual sheets, shows O–H $\cdots$ O distances from 2.67 to 2.74 Å which are in the range of clear hydrogen bonds. Though the geometry of the $H_2O$ molecule was moderately restrained during the refinement procedure, the results are thought to be appropriate for further discussion.

The strong absorptions in the 3500–2800 $cm^{-1}$ region and in the 1680–1600 $cm^{-1}$ region are due to the stretching and bending vibrations of the structurally bound water (Table 6). Measurements in the region of the OH combination modes give no indications for the presence of structural OH groups. The $H_2O$ molecule, belonging to the point group $C_{2v}$, has three normal modes, two stretching (asymmetric $\nu_3$ and symmetric $\nu_1$) and one bending vibration ($\nu_2$). The additional separation of the bands can be attributed to the locally different cation occupation of the *M* positions coordinating the O10 donor and the O8 and O2 acceptor

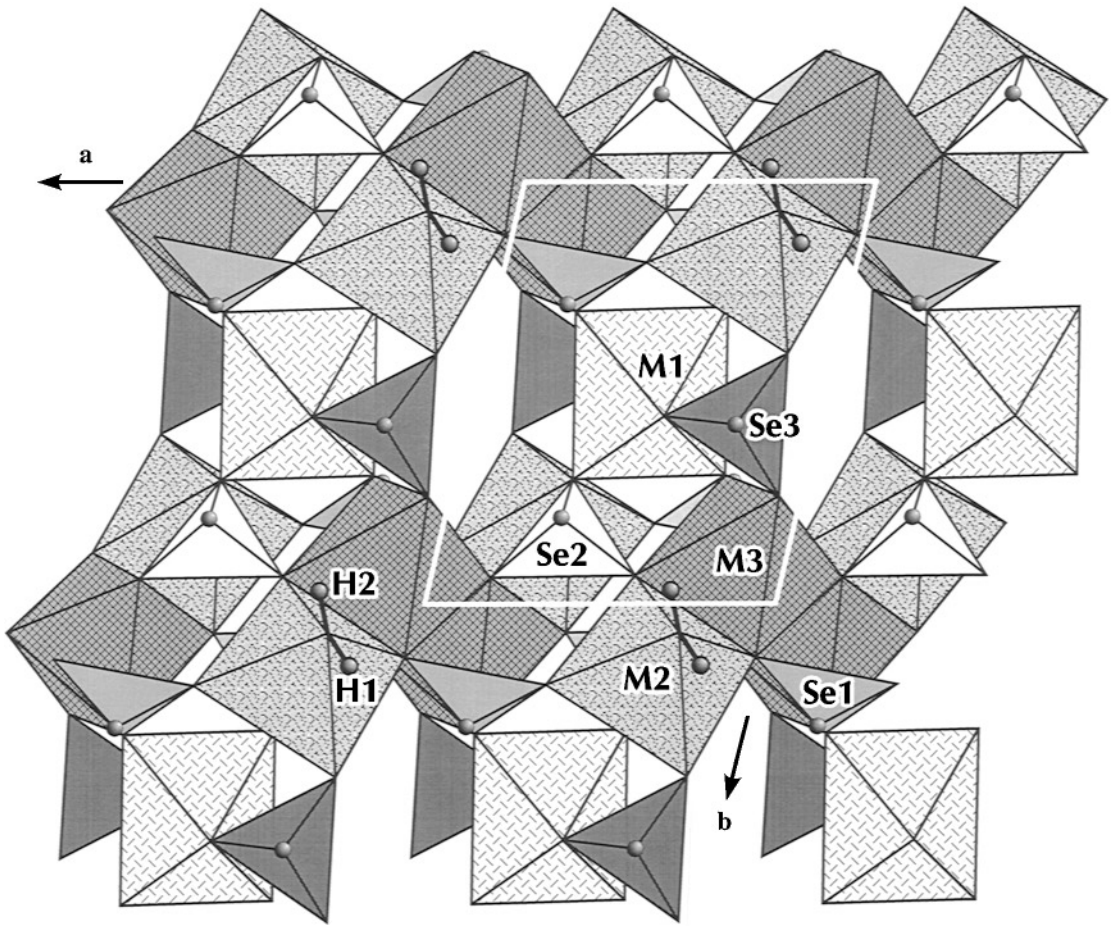


**FIG. 4.** Crystal structure of MGFE in a projection along [001]. The drawings are done with the program ATOMS (11).

oxygens. Band broadening is partially a result of overlapping ($\nu_3 + \nu_1$) bands but is also indicative for a range of slightly varying environments for the $H_2O$ molecule; this is in coincidence with the relatively high displacement parameters (Table 2) of the O10 atom. The position of the absorption maxima of the stretching vibrations is clearly correlated to the length of the hydrogen bond. The "mean" O–H $\cdots$ O distances, 2.733 Å for MGFE, 2.703 Å for COFE, and 2.689 Å for NIFE, are in good agreement with the wavenumber relation diagram given by Ref. (12). Considering the $H_2O$ bending vibration region ($\nu_2$), the significantly higher wavenumber in MGFE (Table 6) is in coincidence with the larger H–O–H angle (Table 8). It is important to state that band separation of the $H_2O$ vibrations can be observed only in single-crystal spectra; powder spectra simply show nonstructured broad-band absorptions.

No definite explanation can be given for the weak absorptions in the 1400–1000 $cm^{-1}$ region. Probably these bands, which are clearly observable only in single-crystal spectra, are overtones and/or combination modes of low-energy "lattice vibrations."

Because of the extremely strong absorptions in the selenite group frequency range of the single-crystal spectra, KBr pellets were prepared for the spectroscopic characterization of the ($SeO_3$) vibrations. The four normal modes of ($SeO_3$) as a pyramidal four-atom group, belonging to point group $C_{3v}$, are all infrared active (13). Within the measured spectral range, symmetric ($\nu_1$) and asymmetric ($\nu_3$) stretching vibrations can be observed. The absorption band at the low energy end of the spectrum is caused by the symmetric bending vibration $\nu_2$ of the ($SeO_3$) groups. In the present compounds, $\nu_1$ and $\nu_3$ vibrations cannot be clearly distinguished. The absorption band at a relatively constant wavenumber of 815 $cm^{-1}$ in all three compounds (Table 6) is attributed to the $\nu_1$ vibration of the ($SeO_3$) groups; three further band maxima at lower energy are attributed to the $\nu_3$ vibration. These bands are probably correlated to the three crystallographically different ($SeO_3$) groups within the structure. Comparing the three compounds it is obvious that the $\nu_3$ absorptions of the ($SeO_3$) groups in MGFE show the weakest extent of band separation but with band maxima at the highest wavenumbers. This is explained by the fact

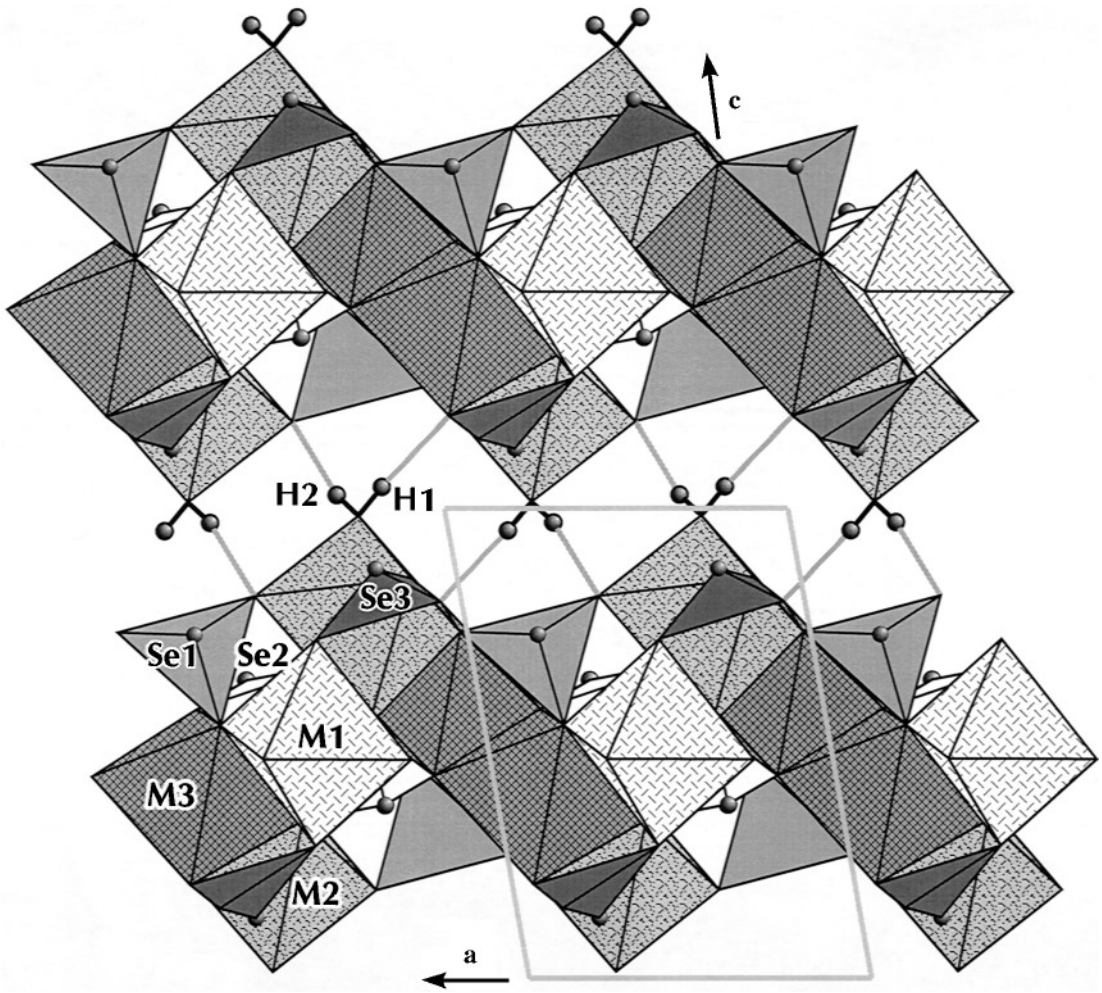


**FIG. 5.** Crystal structure of MGFE in a projection along [010].

that the Se–O distances in MGFE are the shortest and reveal the greatest variability. The COFE compound with minor variations in the Se–O distances (Table 3) shows absorption maxima at the lowest energy.

Distinct absorptions in the range from 530 to 490 $cm^{-1}$ are due to superposed *M*–O stretching vibrations of the sixfold coordinated metal ions. The band position is correlated to the overall mean *M*–O distance; the shortest mean *M*–O distance in NIFE is correlated to the highest wavenumber position.

**TABLE 8**
**The Hydrogen Bonding System in MGFE, COFE, and NIFE**

| | MGFE | COFE | NIFE |
|---|---|---|---|
| O10–H1 | 0.86(6) | 0.90(7) | 0.90(12) |
| O10–H2 | 0.88(5) | 0.90(6) | 0.89(8) |
| H1–O10–H2 | 115(6) | 107(8) | 107(11) |
| O10–O8 | 2.735(6) | 2.676(11) | 2.672(8) |
| O10–O2 | 2.730(5) | 2.730(10) | 2.705(8) |
| O10–H1 ⋯ O8 | 161(7) | 142(12) | 175(15) |
| O10–H2 ⋯ O2 | 158(6) | 147(8) | 149(12) |

## ACKNOWLEDGMENTS

The authors thank Professor J. Zemann for valuable discussions. Dr. M. Götzinger and Dr. F. Brandstätter kindly performed the chemical analyses. Partial financial support was provided by the JCPDS/ICDD under Grant-in-Aid 90-03 to Professor E. Tillmanns.

## REFERENCES

1. G. Giester, *Z. Anorg. Allg. Chem.* **622,** 1788 (1996).
2. M. Wildner, and G. Giester, *Z. Kristallogr., Suppl. Issue No.* **9,** 249 (1995).
3. G. Giester, *Mh. Chem.* **127,** 347 (1996).

4. G. Giester, *Acta Chem. Scand. A* **49,** 824 (1995).
5. G. Giester, *Acta Chem. Scand. A* **51** (1997).
6. M. Wildner, *Mh. Chem.*, **122,** 585 (1991).
7. G. M. Sheldrick, "SHELX-86, A Program for the Solution of Crystal Structures," Univ. Göttingen, Germany, 1986.
8. G. M. Sheldrick "SHELXL-93, A Program for Crystal Structure Refinement," Univ. Göttingen, Germany, 1993.
9. D. Barb, "Grundlagen und Anwendung der Mössbauerspektroskopie," p. 467. Akademie Verlag, Berlin, 1980.
10. W. Lottermoser, P. Kaliba, and K. Forcher, "MOESALZ: A Computer Program for the Evaluation of Mössbauer Spectra." Univ. Salzburg, Austria, 1992.
11. E. Dowty, ATOMS for Windows 3.1, A Computer Program for Displaying Atomic Structures." Kingsport, TN, 1995.
12. A. Novak, *in*: Structure and Bonding, (J. D. Dunitz *et al*., Eds.), Vol. 18, pp. 177–216. Springer, Berlin/Heidelberg/New York, 1974.
13. K. Nakamoto, "Infrared and Raman Spectra of Inorganic and Coordination Compounds," p. 448. Wiley, New York, 1978.